Dwell time algorithm in ion beam figuring

Jian Fen Wu,[1,2,*] Zhen Wu Lu,[2] Hong Xin Zhang,[2] and Tai Sheng Wang[1,2]

[1]Changchun Institute of Optics, Fine Mechanics and Physics, Chinese Academy of Sciences, Changchun 130033, China

[2]Graduate School of Chinese Academy of Sciences, Beijing 100039, China

*Corresponding author: wjf_85@163.com

Received 19 March 2009; revised 12 June 2009; accepted 15 June 2009;
posted 29 June 2009 (Doc. ID 108900); published 2 July 2009

To get a high-precision optical surface, the deconvolved process of dwell time was transferred to a matrix equation in which the damped factor and the extra removal amount were introduced to expand the freedom of solution. A path weight factor and a surface error weight factor were used to take the scanning path and the initial surface error into account. Combined with the Gerchberg bandlimited extrapolation algorithm for initial surface error map extension, a high-precision final surface could be obtained within a factual aperture. Two surface error maps were calculated to rms = 0.1 nm from rms = 130.23 nm and to rms = 0.08 nm from rms = 282.74 nm. The simulations show that a perfect dwell time solution could be obtained by the revised matrix equation and initial surface error map extension with the help of the least squares QR (LSQR) algorithm.

OCIS codes: 220.0220, 220.4610, 220.4000.

1. Introduction

The development of optical technology has increased the requirements for high-precision optical surfaces. At present, the contact figuring methods are limited to obtaining optical surfaces with accuracies down to the nanometer or subnanometer level due to the wear tool, edge effects, and load press. Ion beam figuring (IBF) avoids these problems because of noncontact figuring. More attention has been paid to this technology during the past two decades [1–5]. The principle of IBF is that the computer controlled five-axis moving system moves an ion beam source according to a predefined scanning path and computed dwell time on the optical surface, and the desired removal amounts can be removed by sputtering between the ion beam and the optical material. When the ion beam source is stable and the five-axis moving system is high precision, the desired removal amounts can be expressed as the convolution operation of dwell time function and ion beam removal function [6,7]. The dwell time solution becomes the key approach to ensure the high-precision surface after IBF. In this paper, the deconvolved process was transferred to a matrix equation. The damped factor and extra removal amount are introduced to the matrix equation to expand the freedom of dwell time. Path weight factor and surface error weight factor are introduced to the matrix equation to take the scanning path and initial surface error into account. With the Gerchberg bandlimited extrapolation algorithm for initial surface error map extension, a high-precision surface could be obtained within a factual aperture.

2. Analysis of the Ion Beam Figuring Process

Figure 1 shows the classical sketch of an IBF process [8]. The scanning path and dwell time could be realized by a five-axis moving system. The error amounts are removed by sputtering between the ion beam and the optical material. For a given point, the material removal amounts are proportional to the intensity of the ion beam and the dwell time. The figuring process could be expressed as

$$R_d(x,y) = A(x,y) * * t_c(x,y), \tag{1}$$

where $R_d(x,y)$ is the desired removal function and $A(x,y)$ is the ion beam removal function per unit

0003-6935/09/203930-08$15.00/0

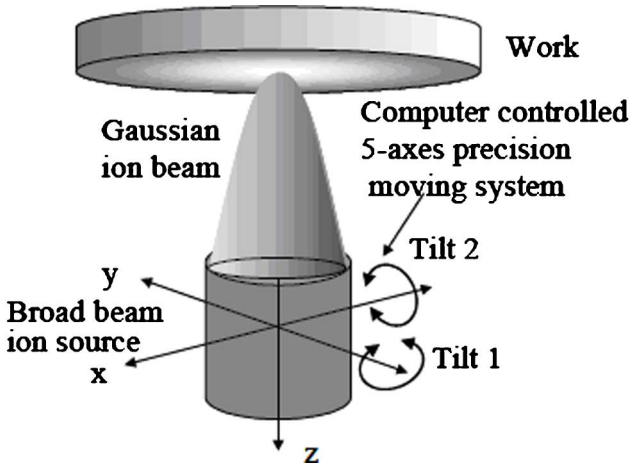

Fig. 1. (Color online) Sketch of IBF process.

time. They are measured before the IBF process. $t_c(x,y)$ is the computed dwell time function.

A. Ion Beam Removal Function

The removal capability characteristic of an IBF process can be described by the ion beam removal function (BRF), $A(x,y)$, which is defined as the material removal profile or "footprint" generated by the projected ion beam per unit time. It can be thought that the ion beam is perpendicularly projected to the plat surface if the curvature radius of the dwell point of the optical surface is far larger than the ion beam radius. Thus we can think that the ion beam removal function is unchangeable across the whole surface in the figuring process, or as figuring on a plat surface. Based on stable ion source technology, it is typically smooth, symmetric, and highly Gaussian in shape and can be described as $A(r) = A_0 \exp(-r^2/\sigma^2)$ with polar coordinates. The peak removal rate A_0, ion beam diameter $d = 6\sigma$, and full width at half-maximum $\mathrm{FWHM} = 2\sigma(\ln 2)^{1/2}$ are the key parameters used to describe the BRF.

B. Desired Removal Function

The desired removal function can be found by subtracting the final desired height of the surface error map from the initial height map:

$$R_d(x_k,y_k) = Z_m(x_k,y_k) - Z_d(x_k,y_k), \qquad (2)$$

where $k = 1,2....N_r$, and N_r denotes the total number of sample points of the surface error map. $Z_m(x_k,y_k)$ and $Z_d(x_k,y_k)$ are the measured and desired heights of sample point (x_k,y_k).

C. Dwell Time Algorithm

There are several methods used to perform the deconvolution operation, such as the Fourier transform, the iterative method, and the matrix method. In a Fourier transform, the same sample interval across the surface error map is needed, and a variable parameter is needed to ensure nonnegative dwell time [6,7]. In the iterative method, the dwell time is made of the desired removal function with some scale and is introduced to the convolution operation to obtain the computed removal function. The difference between the results of convolution and the desired removal function is then used for successive iterations, and the computation is repeated until the result converges to within an acceptable limit of error. However, experience indicates that this method is not always stable and sometimes fails to converge [9]. The matrix approach [10], in which the sample interval can be arranged freely, transfers the deconvolving process into a matrix equation. Unfortunately, the matrix equation is generally an ill-posed equation and is susceptible to the trivial changes of the matrix. Even if the dwell time could be solved, the results are both positive and negative and could not be used with the IBF process directly. To solve this problem, a damped factor was introduced to the matrix equation to balance the relation between the residual surface errors and the magnitude of the dwell time [10]. However, simulations based on the matrix approach show that a high-precision surface could not be obtained with the unique damped factor.

3. Revised Dwell Time Matrix Equation

In this section, the deconvolved matrix equation is first set up. The damped factor and extra removal amount are introduced to the matrix equation to expand the freedom of dwell time. The path weight factor and the surface error weight factor are used to take scanning path and surface error into account.

A. Setup of Matrix Equation

When the ion beam scans all the dwell grids on an optical surface, the actual material removal amounts on a given point can be described as

$$R_a(x_k,y_k) = \sum_{i=1}^{N_t} A(x_k - \xi_i, y_k - \eta_i) t_c(\xi_i,\eta_i), \qquad (3)$$

where N_t is the total numbers of ion beam dwell points. $A(x_k - \xi_i, y_k - \eta_i)$ is the material removal amount per unit time at point (x_k,y_k) when the center of the ion beam dwell is on the point (ξ_i,η_i), and $t_c(\xi_i,\eta_i)$ is the dwell time. With the help of

$$R_a(x_k,y_k) = r_{a_k}, \qquad R_d(x_k,y_k) = r_{d_k},$$
$$A(x_k - \xi_i, y_k - \eta_i) = a_{ki}, \qquad t_c(\xi_i,\eta_i) = t_i,$$

Eq. (3) can be expressed as

$$\begin{pmatrix} r_{a_1} \\ r_{a_2} \\ \vdots \\ r_{a_{N_r}} \end{pmatrix} = \begin{pmatrix} a_{11} & a_{12} & \cdots & a_{1N_t} \\ a_{21} & a_{22} & \cdots & a_{2N_t} \\ \vdots & \vdots & \vdots & \vdots \\ a_{N_r1} & a_{N_r2} & \cdots & a_{N_rN_t} \end{pmatrix} \begin{pmatrix} t_1 \\ t_2 \\ \vdots \\ t_{N_t} \end{pmatrix}. \qquad (4)$$

We let the left vector of Eq. (4) equal the desired removal function; the deconvolution operation of dwell time would then become the solution of the matrix equation. The dwell and sample grids of optical surface could be freely arranged according to scanning path and initial surface error map. The root mean square (rms) of residual surface error could be described as rms $= \{\sum_{k=1}^{N_r}[\sum_{i=1}^{N_t}(a_{ki}t_i - r_{d_k})]^2/N_r\}^{1/2}$.

B. Revised Matrix Equation

The unique dwell time solution of Eq. (4) could be computed by the inverse matrix method when the rank $(A) = N_r = N_t$. However, matrix A is generally singular and susceptible to trivial changes. The results are both positive and negative and could not be used in the IBF process directly. As to $N_t < N_r$, the rank of matrix A might not equal the rank of its extending matrix in engineering. So it is not advisable to find the accuracy solution of matrix equation (4) in engineering. A damped factor W was introduced to Eq. (4) [10]:

$$\begin{pmatrix} r_{d_1} \\ r_{d_2} \\ \vdots \\ r_{d_{N_r}} \\ 0 \\ 0 \\ \vdots \\ 0 \end{pmatrix} = \begin{pmatrix} a_{11} & a_{12} & \cdots & a_{1N_t} \\ a_{21} & a_{22} & \cdots & a_{2N_t} \\ \vdots & \vdots & \ddots & \vdots \\ a_{N_r1} & a_{N_r2} & \cdots & a_{N_rN_t} \\ W & 0 & \cdots & 0 \\ 0 & W & \cdots & 0 \\ \vdots & \vdots & \ddots & \vdots \\ 0 & 0 & \cdots & W \end{pmatrix} \begin{pmatrix} t_1 \\ t_2 \\ \vdots \\ t_{N_t} \end{pmatrix}, \quad (5)$$

$[t_1, t_2, \ldots t_{N_t}]^T$ of Eq. (5) should minimize the following expression:

$$\left\{\sum_{k=1}^{N_r}\left[\sum_{i=1}^{N_t}(a_{ki}t_i - r_{d_k})\right]^2/N_r + W^2\sum_{i=1}^{N_t}t_i^2\right\}^{1/2}. \quad (6)$$

Because the deconvolution operation of dwell time could be transferred to Eq. (5) with the ion beam removal function, the initial surface error map, and the scanning path in the individual IBF process, then the damped factor is a parameter for the individual IBF process. In fact, the damped factor, with the range of 0 to $\times\ \infty$, is a weight factor that allows the user to specify the relative weight between the residual surface error and the magnitude of the dwell time solution. Simulations show that it is hard to get the nonnegative dwell time solution with a small damped factor; however, the larger damped factor may result in larger residual errors due to a relatively small weight. The problem now is how to find the suitable damped factor to balance the relation between them and at the same time to ensure the nonnegative dwell time solution. We proposed a method to revise Eq. (5). Except for the damped factor, the extra removal amount is introduced to expand the freedom of solution. The effects of scanning path and initial surface error on the final surface are also taken into account with path weight factor and surface error weight factor. Thus Eq. (5) becomes

$$\begin{pmatrix} r_{d_1} + \gamma_0 \\ r_{d_2} + \gamma_0 \\ \vdots \\ r_{d_{N_r}} + \gamma_0 \\ 0 \\ 0 \\ \vdots \\ 0 \end{pmatrix} = \begin{pmatrix} a_{11} & a_{12} & \cdots & a_{1N_t} \\ a_{21} & a_{22} & \cdots & a_{2N_t} \\ \vdots & \vdots & \ddots & \vdots \\ a_{N_r1} & a_{N_r2} & \cdots & a_{N_rN_t} \\ WP_1S_1 & 0 & \cdots & 0 \\ 0 & WP_2S_2 & \cdots & 0 \\ \vdots & \vdots & \ddots & \vdots \\ 0 & 0 & \cdots & WP_{N_t}S_{N_t} \end{pmatrix} \begin{pmatrix} t_1 \\ t_2 \\ \vdots \\ t_{N_t} \end{pmatrix}, \quad (7)$$

where matrix A was extended to an $(N_r + N_t) \times N_t$ matrix, and the desired removal vector was extended to an $(N_r + N_t) \times 1$ column vector. The column vectors of matrix A and desired removal vector are not correlated with each other. This is always true in engineering no matter what the scanning path and initial surface error map. Then Eq. (5) becomes a completely rank-deficient least squares problem, in which the trivial changes of matrix A would not have significant effects on the solution. The solution $\vec{t} =$ where W is still the damped factor, and γ_0 is the extra removal amount. The dwell time solution is mainly responsible for the two variants. The path weight factor can be described as

$$P_i = H \cdot \sum_{j=1}^{N_t} A(\xi_i - \xi_j, \eta_i - \eta_j) / \sum_{i=1}^{N_t}\sum_{j=1}^{N_t} A(\xi_i - \xi_j, \eta_i - \eta_j). \quad (8)$$

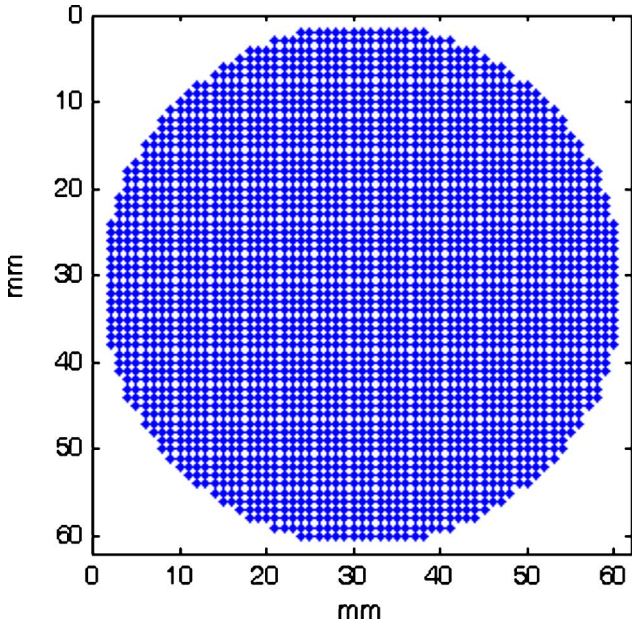

Fig. 2. (Color online) Scanning dwell grids according to uniform scanning path (extending half of the ion beam diameter).

When the ion beam scans all dwell grids according to the scanning path per unit time, the removal amount on dwell point (ξ_i, η_i) is $\sum_{j=1}^{N_t} A(\xi_i - \xi_j, \eta_i - \eta_j)$. Thus the normalized path weight factor P_i can be obtained by Eq. (8). It can be imaged that P_i is larger in dense grid areas than in sparse grids. When P_i was introduced to Eq. (7), it revised the relative weight between the residual surface error and the magnitude of the dwell time solution. Thus the effects of scanning path grids on the final surface could be taken into account with P_i. It is especially helpful for an irregular scanning path. The surface error weight factor can be described as

$$S_i = [(R_d + \gamma_0)_{\max} - (R_d(\xi_i, \eta_i) + \gamma_0)]/(R_d + \gamma_0)_{\max}. \tag{9}$$

The desired removal amount on dwell point (ξ_i, η_i) is $R_d(\xi_i, \eta_i) + \gamma_0$, which can be inverted and normalized by Eq. (9). It can be imaged so that S_i is larger in small rather than large desired removal amount points. When S_i was introduced to Eq. (7), it revised the relative weight between the residual surface error and the magnitude of the dwell time solution. Thus the effects of the initial surface error map on the final surface could be taken into account with S_i.

The dwell time solution of Eq. (7), $\vec{t} = [t_1, t_2, \ldots t_{N_t}]^T$, should minimize the following expression:

$$\left\{ \sum_{k=1}^{N_r} \left[\sum_{i=1}^{N_t} (a_{ki} t_i - r_{d_k} - \gamma_0) \right]^2 / N_r + W^2 \sum_{i=1}^{N_t} P_i^2 S_i^2 t_i^2 \right\}^{1/2}. \tag{10}$$

Relative to Eq. (5), γ_0 expands the freedom of dwell time. P_i and S_i revised the weight between the residual surface error and the magnitude of dwell time. The singular value decomposition (SVD) can be used to find the minimum least-squares solution of Eq. (7), $\vec{t}_{\mathrm{SVD}} = [t_1, t_2, \ldots t_{N_t}]^T$:

$$\vec{pst}_{\mathrm{SVD}} = \sum_{i=1}^{M} \frac{\sigma_i \vec{\mu}_i^T (\vec{r}_d + \vec{\gamma}_0)}{\sigma_i^2 + W^2} \vec{\nu}_i, \tag{11}$$

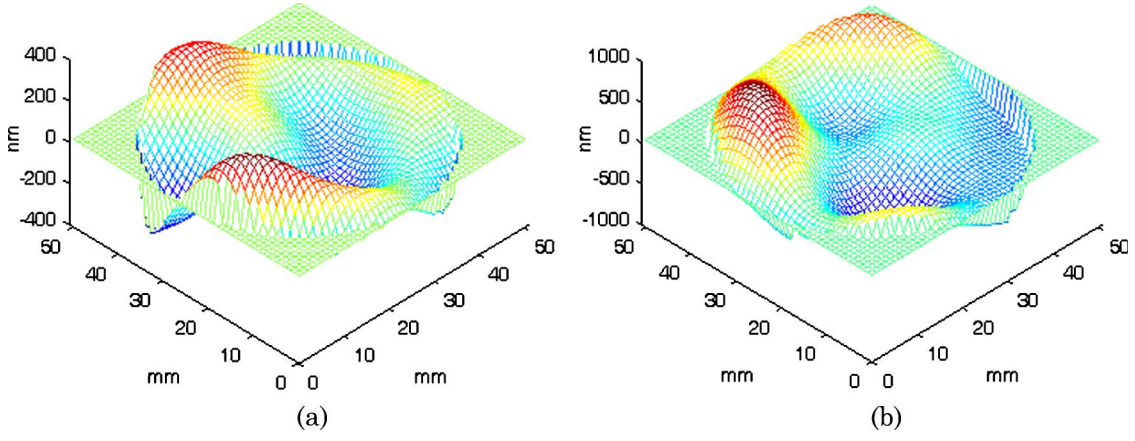

Fig. 4. (Color online) Initial surface error maps on (a) the flat surface and (b) the parabolic surface.

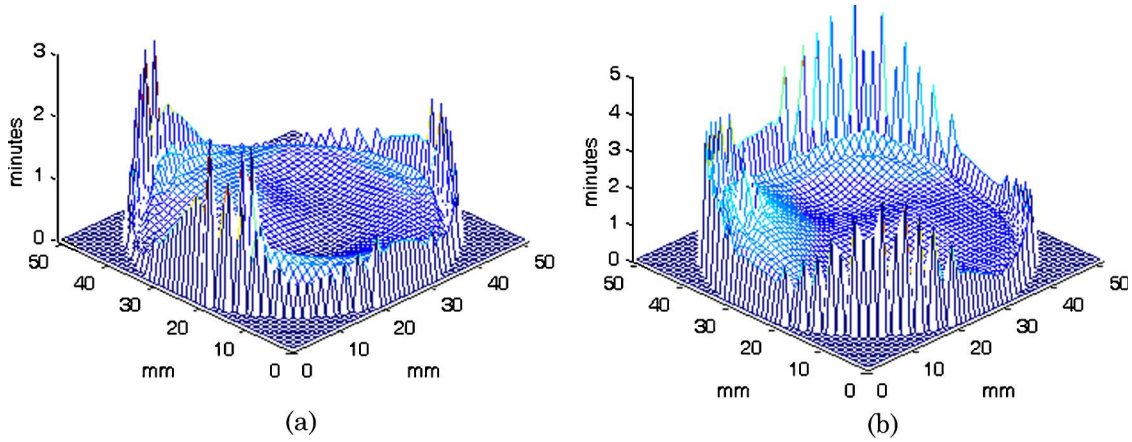

Fig. 5. (Color online) Dwell time without extension on (a) the flat surface and (b) the parabolic surface.

where $\vec{pst}_{\mathrm{SVD}} = [P_1 S_1 t_1, P_2 S_2 t_2, \ldots P_{N_t} S_{N_t} t_{N_t}]^T$, M is the singular value numbers of matrix A, and $\vec{\mu}_i$ and $\vec{v}_i$ are the ith left singular and ith right singular orthonormal column vectors. From Eq. (11), we can see that γ_0 would make the dwell time solution move toward the positive direction as a whole, and the dwell time solution of Eq. (5) with some negative will become positive in Eq. (7). The range of the dwell time solution enlarges relative to that of Eq. (5). Thus we could find the nonnegative dwell time solution with smaller damped factor by the help of γ_0. For obtaining a high-precision surface, there are generally many dwell points and surface error sample points. The diameter of the ion beam is smaller than the diameter of the optical component. Because of these facts, matrix A becomes a large-scale sparse matrix, and SVD is not a good method due to the long time to compute. A numerical algorithm, known as least squares QR (LSQR) [11], has been developed that addresses the problem of solving a large, sparse, rank-deficient system of equations. With the reasonable range of W and γ_0, the dwell time solution $\vec{t}_{\mathrm{LS}} = t(W, \gamma_0)$ can be obtained from Eq. (7). The residual surface error could be expressed as the function of W and γ_0: $\mathrm{rms} = \left\{\sum_{k=1}^{N_r}\left[\sum_{i=1}^{N_t}(a_{ki} t_{i_{\mathrm{LS}}} - r_{d_k} - \gamma_0)\right]^2 / N_r\right\}^{1/2}$.

Based on the LSQR algorithm for Eq. (7), the time cost is several minutes, so the damped factor and extra removal amount can be decided by trial and error for an individual IBF process. Usually the damped factor is less than 10, and the extra removal amount is less than half of the wavelength. W and γ_0 should meet the following criteria: (a) Dwell time solutions $\vec{t}_{\mathrm{LS}}$ are nonnegative. (b) The magnitude norm of $\vec{t}_{\mathrm{LS}}$, $\|\vec{t}_{\mathrm{LS}}\|_2^2$, should be bound to a given value. (c) Based on the above, the suitable values of W and γ_0 can be found by the residual surface error, $\mathrm{rms} = f(W, \gamma_0)$, meeting the precision requirements.

4. Initial Surface Error Map Extension

A. Initial Surface Error

Although final surface precision is guaranteed by the dwell time solution computed by the revised Eq. (7), simulations show that residual surface error is larger at the edge than in the center, and the dwell time has a spiky shape at the edge. The main reason is the discontinuity of the initial surface error map at the edge. Different from edge effects in contact figuring, IBF is a noncontact figuring method. The ion beam removal function is unchangeable whether the optical component exists or not. This fact provides us a

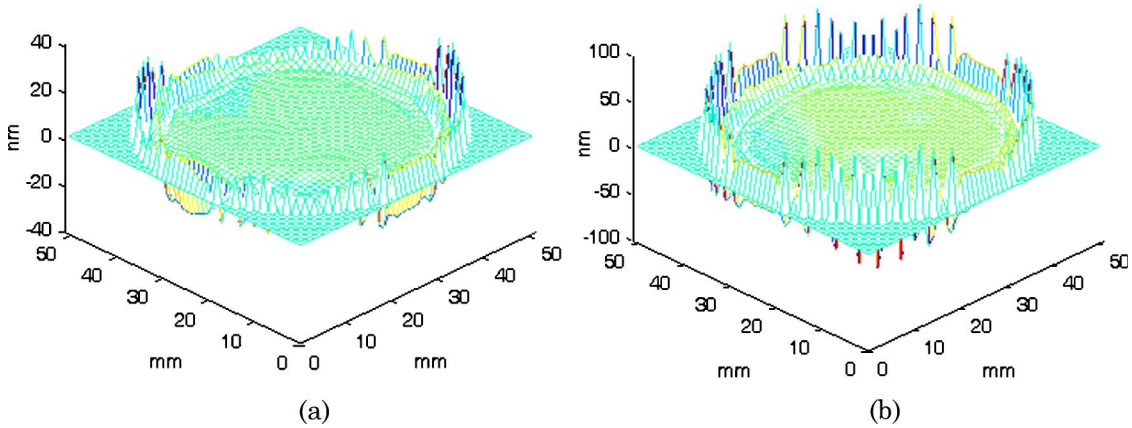

Fig. 6. (Color online) Residual surface error maps after IBF on (a) the flat surface and (b) the parabolic surface.

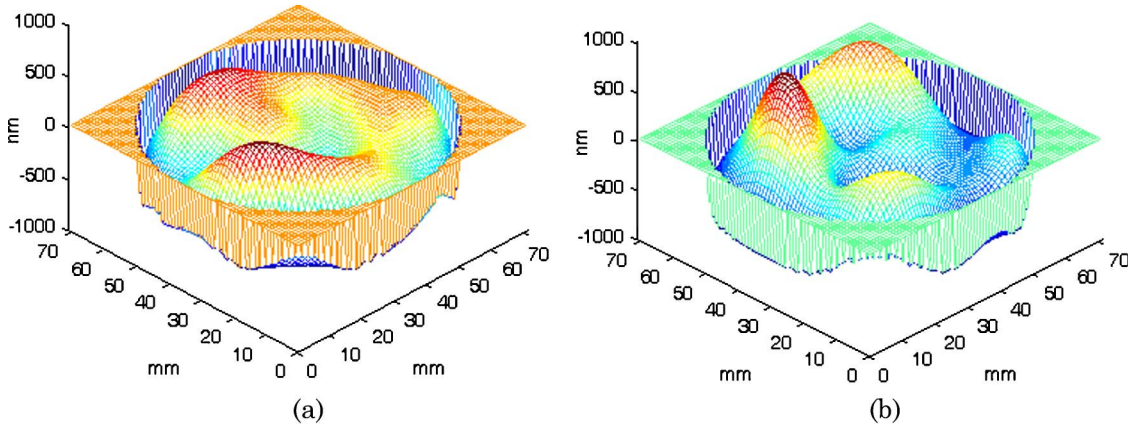

Fig. 7. (Color online) Initial surface error maps extending an ion beam diameter on (a) the flat surface and (b) the parabolic surface.

method to deal with the problems mentioned above. We extend the initial surface error map with an ion beam diameter and make the extension part join smoothly with the factual part. The new extended surface error map is regarded as the initial surface error that needs to be figured. Thus the desired removal function and dwell time will also extend an ion beam diameter. However, we just take care of the factual initial surface error part. Because the outer spiky dwell time at half of the ion beam diameter has no difference on the factual initial surface error part, it can be abandoned. The left dwell time that extends half of the ion beam diameter becomes smooth at the edges, and the final surface will also be smooth within a factual aperture.

B. Gerchberg Bandlimited Extrapolation Algorithm [12]

The Gerchberg bandlimited extrapolation algorithm in two dimensions was used to extend the factual surface error map. Here $u(x,y)$ denotes the initial surface error map that is nonzero over region T_{xy}, and the extended region is denoted by T_{xy0}. We let $u(x,y)$ have a Fourier spectrum $U(f_x,f_y)$ after extension, and we define the bandlimited spectrum region as $\Omega_{f_xf_y}$. Here $G_{T_{xy}}$, $G_{T_{xy0}}$, and $G_{\Omega_{f_xf_y}}$ are gate functions defined in regions T_{xy}, T_{xy0}, and $\Omega_{f_xf_y}$, respectively. Then we can show the initial surface error map $u(x,y)$ after extension:

$$u_N(x,y) = \sum_{n=0}^{N} H^n u(x,y) G_{T_{xy0}}; \tag{12}$$

here $H = (G_{T_{xy0}} - G_{T_{xy}})F^{-1}G_{\Omega_{f_xf_y}}F$ is the extension operator, and F and F^{-1} are Fourier transform and Fourier inverse transform. It has been proved that $u_N(x,y)$ will converge to $u(x,y)$ with bandlimited region $\Omega_{f_xf_y}$ as $N \to \infty$ [12]. In engineering, Eq. (10) is run to some N to ensure a smooth joint at the edge.

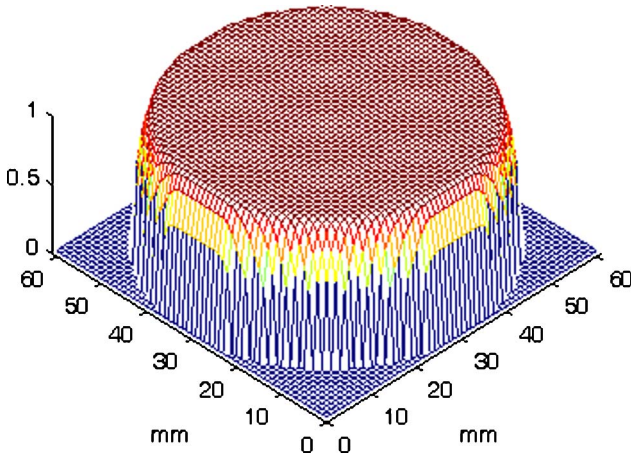

Fig. 8. (Color online) Path weight factor map according to a uniform scanning path (extending half of the ion beam diameter).

5. Simulations

Two simulations are conducted to demonstrate how to solve the dwell time mentioned above. The parameters of the ion beam removal function are $A_0 = 100\,\text{nm/min}$, $d = 10\,\text{mm}$, and FWHM $= 2.7752\,\text{mm}$. Ion beam scanning dwell grids according to the scanning path are linear uniform intervals (1 mm) in the projected X–Y plane, and the dwell point numbers are the same as the surface error sample point numbers. Figure 2 shows the scanning dwell grids according to the scanning path. Figure 3 shows the ion beam removal function per unit time. Figure 4 shows the initial surface error maps of two optical components with a diameter of 50 mm in which (a) shows a flat component and (b) shows a parabolic component with vertex radius 500 mm (it is far larger than the ion beam radius). The initial surface errors are rms $= 130.23\,\text{nm}$, PV $= 596.98\,\text{nm}$, and rms $= 282.74\,\text{nm}$, PV $= 1316.92\,\text{nm}$, respectively. To demonstrate the method mentioned above, the desired removal function was first computed by subtracting the negative minimum of the initial error height map of the optical surface from it and introduced to Eq. (5). The results show that the nonnegative dwell time can be guaranteed with $W = 1.2$ and $W = 1.4$ for flat and parabolic optical components, respectively. The residual surface error is rms $= 41.7\,\text{nm}$, PV $= 119.03\,\text{nm}$, and rms $= 118.52\,\text{nm}$, PV $= 244.2\,\text{nm}$, respectively. It can be seen that the

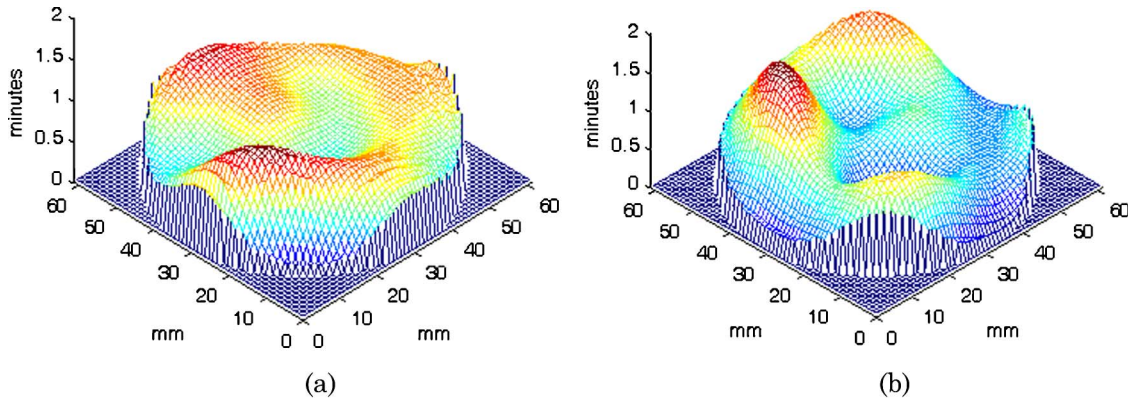

Fig. 9. (Color online) Dwell time extending half of the ion beam diameter on (a) the flat surface and (b) the parabolic surface.

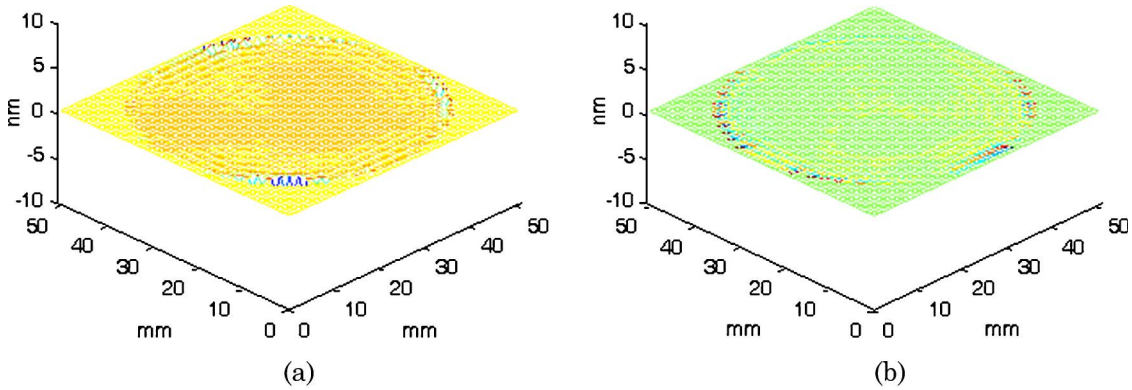

Fig. 10. (Color online) Residual surface error maps within a factual aperture after IBF on (a) the flat surface and (b) the parabolic surface.

residual surface errors are not greatly improved. We can state that the high-precision final surface could not be guaranteed with a unique damped factor in engineering. Based on the method mentioned above, the path weight factor and the surface weight factor computed with Eqs. (8) and (9), and the extra removal amounts $\gamma_0 = 63.28$ nm and $\gamma_0 = 126.56$ nm are introduced in Eq. (7) for flat and parabolic optical components. With the help of the LSQR algorithm, the nonnegative dwell time solutions could be found with $W = 0.35$ and $W = 0.3$. The residual surface error is rms $= 4.11$ nm, PV $= 56.76$ nm, and rms $=$ 16.58 nm, PV $= 136.18$ nm, respectively. It can be seen that the residual surface errors are greatly improved relative to the results with the unique damped factor. Figure 5 shows the dwell time solutions, and Fig. 6 shows the residual surface error maps after IBF. It is obvious that the revised Eq. (7) can be used to find a perfect dwell time solution that ensures the final surface precision is at a good level. However, it also can be seen that both the dwell time and the residual surface error has a spiky shape at edges, and residual surface errors are higher at edges than centers, as shown in Figs. 5 and 6. Due to the acceptable ranges of velocity and acceleration for the five-axis moving system, the spiky dwell time should be checked to meet requirements before application to a practical system. The residual surface error difference between center and edge is also unfavorable for figuring stitching optical components. As discussed in Section 4, the Gerchberg extrapolation algorithm was used to extend initial surface error maps to an ion beam diameter, as shown in Fig. 7. Extra removal amount $\gamma_0 =$ 63.28 nm and path weight factor and surface weight factor were introduced to Eq. (7). Because of the same scanning path, the path weight factor is the same for the two simulations, as shown in Fig. 8. Based on the LSQR algorithm, the nonnegative dwell time solution can be obtained with a smaller damped weight factor $W = 0.02$ for two components. As stated in Subsection 4.A, the dwell time extended at half of the ion beam diameter becomes smooth at the edges, as shown in Fig. 9. The residual surface error will also be smooth within a factual aperture, as shown in Fig. 10. They are perfectly reduced to rms $=$ 0.1 nm, PV $= 1.9$ nm, and rms $= 0.08$ nm, PV $=$ 1.39 nm, respectively. All these demonstrate that a high-precision final surface could be realized by the combination of initial surface error map extension and revised matrix equation (7) with the help of the LSQR algorithm.

6. Conclusion

The deconvolved process of dwell time was transferred to a revised matrix equation, in which the

damped factor and the extra removal amount were introduced to expand the freedom of dwell time, and the path weight factor and surface error weight factor were introduced to take scanning path and initial surface error into account. Combined with the Gerchberg bandlimited extrapolation algorithm for initial surface error map extension, a high-precision final surface could be obtained within a factual aperture. The simulations of 50 mm diameter flat and parabolic optical components show that the residual surface errors were ideally reduced to rms $= 0.1$ nm and rms $= 0.08$ nm, respectively. The conclusion is that a perfect dwell time could be obtained by the combination of initial surface error map extension and revised matrix equation (7) with the help of the LSQR algorithm. The method in this paper can be used to instruct the IBF process perfectly.

This work was supported by the National Natural Science Foundation of China (NNSF) grant 10704072.

References

1. N. A. Lynn, E. K. Robert, and S. L. Timothy, "Surface error correction of a Keck 10 m telescope primary mirror segment by ion figuring," Proc. SPIE **1531**, 195–204 (1991).
2. P. M. Shanbhag, M. R. Feinberg, G. Sandri, M. N. Horenstein, and T. G. Bifano, "Ion-beam machining of millimeter scale optics," Appl. Opt. **39**, 599–611 (2000).
3. L. Aschke, F. Schubert, J. Kegeler, and A. Schindler, "Flatness correction of NZTE mask blank substrates," Proc. SPIE **4343**, 646–653 (2001).
4. M. Ghigo, P. Conconia, M. Sala, E. Antonello, G. Pareschi, and L. Poletto, "Field corrector for the Ultraviolet Italian Sky Surveyor on the International Space Station (UVISS): ion beam figuring and application of the multilayer filters," Proc. SPIE **5488**, 457–480 (2004).
5. T. Hänsel, A. Nickel, and A. Schindler, "Ion beam figuring of strongly curved surfaces with an (x,y,z) linear three-axis system," in *Optical Fabrication and Testing*, OSA Technical Digest (CD) (Optical Society of America, 2008), paper JWD6.
6. S. R. Wilson and J. R. McNeil, "Neutral ion beam figuring of large optical surfaces," Proc. SPIE **818**, 320–322 (1987).
7. S. R. Wilson, D. W. Reicher, C. F. Kranenberg, and J. R. McNeil, "Ion beam milling of fused silica for windows fabrication," Proc. SPIE **1441**, 82–85 (1990).
8. A. Schindler, T. Hänsel, F. Frost, R. Fechner, and G. Seidenkranz, "Ion beam finishing technology for high precision optics production," in *Optical Fabrication and Testing*, A. Sawchuk, ed., Vol. 76 of OSA Trends in Optics and Photonics Series (Optical Society of America, 2002), paper OTuB5.
9. H. Fang, P. Guo, and J. Yu, "Dwell function algorithm in fluid jet polishing," Appl. Opt. **45**, 4291–4296 (2006).
10. C. L. Charles, C. M. Egert, and K. W. Hyltonet, "Advanced matrix-based algorithm for ion beam milling of optical components," Proc. SPIE **1752**, 54–62 (1992).
11. C. Paige and M. A. Saunders, "LSQR: an algorithm for sparse linear equations and sparse least squares," ACM Trans. Math. Software **8**, 43–71 (1982).
12. J. Robert and Marks, "Gerchberg's extrapolation algorithm in two dimensions," Appl. Opt. **20**, 1815–1820 (1981).